Study of the conservation state of European street furniture in painted cast irons

C. Soffritti, L. Calzolari, A. Balbo, F. Zanotto, C. Monticelli, A. Fortini, G.L. Garagnani

This work evaluates the state of conservation of four painted and partially corroded post-mounted luminaries in cast irons, dating back to the nineteenth and the twentieth centuries and coming from foundries located in Italy and France.
The form, distribution and size of graphite in the cast irons were evaluated by optical microscopy, in accordance with the standard EN ISO 945-1:2008. The same technique was also used to determine the constituents of the microstructures. The corrosion attack morphology, the patina stratification and the main corrosion products were characterized by scanning electron microscopy, equipped with variable pressure technology (VPSEM) and energy dispersive spectroscopy (EDS), diffuse reflectance FT-IR (DRIFT) spectroscopy and X-ray diffractometry (XRD).
The protectiveness of the ancient paints was evaluated by electrochemical impedance spectroscopy (EIS). In order to check the reliability of the technique, EIS measurements were also performed on plates in modern gray cast iron with the current standard painting cycle of Neri S.p.A. (Longiano, FC, Italy), during neutral salt spray testing for 83 days (corresponding to 2000 h).
The metallographic analyses showed that the microstructures were consistent with the procedures employed for manufacturing complex shape casting with variable wall thickness. On the corroded surfaces the graphitization of the cast irons was detected. This phenomenon was accompanied by the deposition of thick corrosion layers, containing lepidocrocite, goethite and impurities from the corrosive environment. No historical paints were recognized, suggesting the removal of the deteriorated paint layers, before the application of modern paint systems. Finally, the electrochemical characterization established the poor protectiveness offered by the paints on the post-mounted luminaries.

KEYWORDS: STREET FURNITURE, CAST IRONS, MICROSTRUCTURE, GRAPHITIZATION, PAINTING

INTRODUCTION

In the literature, street furniture was defined for the first time by Baron Haussmann (urbanist, Prefect of Paris, France, from 1853 to 1870 CE) as 'the group of objects or accessories which, installed in the urban space, performs a functional service for the community'. Bassi Neri and Bazzocchi [1] further considered that 'safety, hygiene, comfort and entertainment were the requirements of the nascent bourgeoisie, and the modern city needed to respond to them. The city layout changed radically in those years, making it possible to introduce new purposely-created elements'. Thus, street furniture was a class of objects created to ease life in urban settlements, which has evolved with the human necessities during the years, and nowadays is an integral part of the city. Street lamps, benches, balconies, grids, fountains and gazebos are only some of the elements that compose the whole category and which have an ancient origin [2].
During the second half of the nineteenth century and the first decades of the twentieth century, many items intended for illumination and urban décor, as well as many architectural accessories, were made of cast iron. However, street furniture was not exclusively composed of cast iron: wrought iron was preferred for ornamental manufacturing up to the second half of the eigh-

C. Soffritti, L. Calzolari, A. Balbo, F. Zanotto, C. Monticelli A. Fortini, G.L. Garagnani

"A. Daccò" Corrosion and Metallurgy Study Centre,
Department of Engineering,
University of Ferrara, Via Saragat 1,
I-44122 Ferrara, Italy

teenth century. Over centuries, other materials were also used, such as concrete for street lamps and stone for balconies and grids. Nevertheless, cast iron alloys brought street furniture to a massive diffusion [3].
Atmospheric corrosion of ferrous alloys and deterioration of protective coatings is a serious problem for the safeguard of cultural heritage exposed to the action of natural weathering and urban pollution. Metal corrosion occurs at the surface/moisture film interface and air pollutants and particulate matter, which partially dissolve and ionize in the moisture film, can accelerate it. Solid and/or gaseous pollutants, such as SO_2, NO_x and CO_2, under the effects of O_2, temperature, humidity and sunlight may also react to form new secondary pollutants [4].
Cast irons have good resistance to atmospheric corrosion thanks to more or less corrosion-resistant phases (graphite, phosphorous eutectic and, to a lesser extent, carbides and carbide eutectic) that are largely or completely absent from steel [5]. The rate of atmospheric corrosion of cast iron is lower than that of steel, especially in the presence of high concentrations of pollutants [6]. At relative humidity (RH) lower than ~65%, atmospheric corrosion rates are usually relatively low. However, at RH above ~70%, unalloyed cast irons suffer of generalized corrosion involving the formation of mixtures of oxides and hydrated oxides similar to those in steel. In polluted atmospheres, the corrosion layer also contains sulfates, chlorides and nitrates. These corrosion rates tend to decrease with increasing exposure duration due to the formation of an adherent and highly protective layer of corrosion products [5]. The historical street furniture composed of cast irons was usually exposed to the atmosphere for fifty or even one hundred and more years, but for the majority of its exposure the surfaces were protected by paints with active pigments able to provide cathodic protection or anodic passivation [7]. Corroded surfaces of cast irons tend to crumble and flake: this phenomenon is more evident under the paint layers.
The electrochemical impedance spectroscopy (EIS) is proven to be a useful technique for estimating the rate of atmospheric corrosion of metals [8–12]. It has a great advantage as a non-destructive tool for studying the electrochemical reaction on the metal surface and for identifying cracks and/or porosity on the surface layers.
In the last three decades, EIS has been successfully used for the evaluation of the protective efficiency of organic coatings and its change during exposure to corrosive environments [13] by specially designed monitoring probes, during laboratory tests as well as field trials [14–16]. Letardi et al. performed in situ EIS measurements with a special "contact probe" to determine the effectiveness of some protective coatings applied on artificially patinated coupons and real monuments [17,18]. The same probe arrangement is adopted by Balbo et al. to monitor the corrosion rate, in the presence of synthetic rainwater, of bronze and gilded bronze coupons produced with the ancient techniques employed during the Renaissance period [19]. More recently, solid state probes are designed and used in EIS measurements to evaluate the level of corrosion protection afforded by the paint coating on a steel sculpture (Toku sculpture, Canberra-Nara Peace Park, Canberra, Australia) [20].
Our study evaluates the state of conservation of four painted and partially corroded post-mounted luminaries in cast irons, dating back to the nineteenth and the twentieth centuries and coming from foundries located in Italy and France. The results of the investigations on the cast irons microstructure are presented. Microstructural features are used for evaluating manufacturing procedures. The study of the corrosion attack morphology, the patina stratification and the main corrosion products is also performed to elucidate the corrosion process. Finally, the electrochemical characterization is carried out for estimating the protectiveness of paints applied on the surface of the examined artefacts.

MATERIALS AND METHODS

In order to preserve the objects from further damage, most of the investigations were carried out on fragments collected from the artefacts. A summary of characteristics of the studied fragments, i.e. the origin, the year of manufacturing, the nationality of the foundries, together with the performed experimental procedure (conventional/non-destructive/in situ) are listed in Tab. 1.

Tab. 1 – Summary of the studied fragments with information on year of manufacturing, nationality of the foundries and performed experimental analyses (conventional/non-destructive/in situ). / *Elenco dei frammenti analizzati, con indicazione dell'anno di produzione della nazionalità della fonderia di provenienza e della tipologia di tecnica utilizzata su ciascun frammento.*

			INVESTIGATIONS				
Fragment	**Year**	**Nationality of the foundry**	**Conventional**	**Non-destructive**			**In situ**
			Metallography	SEM/EDS	XRD	FT-IR	EIS
1_Enna	1880-1890	Italy	**x**	**x**		**x**	**x**
2_Bergamo	1900	n.r.	**x**	**x**	**x**	**x**	**x**
3_Imola	1929	Italy	**x**	**x**		**x**	
4_Nice	1930	France	**x**	**x**	**x**	**x**	

n.r. = not reported

The microstructural characterization was performed on some representative fragments obtained from the longitudinal section (sample observed in the direction of the metal surface) and from the cross section (sample observed across the thickness of the metal). The fragments were embedded in cold mounting resin, polished and analyzed by conventional metallographic techniques. The analyses of the cast irons microstructure before chemical etching were carried out by a Leica MEF4M optical microscope (OM) (Leica, Wetzlar, Germany), to determine the form, distribution and size of graphite, in accordance with the standard EN ISO 945-1:2008. The microstructure was analyzed after chemical etching with Nital 4 (4% nitric acid in ethanol) by both optical microscopy and scanning electron microscopy. The scanning electron microscope was a Zeiss EVO MA 15 (Zeiss, Oberkochen, Germany) equipped with an energy dispersive microprobe (EDS), operating in variable pressure conditions (VPSEM).
The patina stratigraphy was investigated on the cross sections, in non-etched conditions, by VPSEM/EDS. The coating thickness was non-uniform and difficult to be correctly estimated due to the degradation conditions. It resulted to be around 200 µm in all cases, with the exception of 2_Bergamo sample which was thinner (about 100 µm). Both paints and corrosion products collected from the fragments were analyzed by diffuse reflectance FT-IR (DRIFT) spectroscopy with a Thermo-Scientific Nicolet iS50 spectrometer (Thermo Fisher Scientific, Waltham, USA). The spectrometer was purged with dry, CO_2-free air generated with a Balston 75-52 unit and a deuterated triglycine sulfate (DTGS) detector was used to investigate the region from 4000-400 cm^{-1} with a resolution of 4 cm^{-1}. Paint samples were obtained by abrading the painted post surfaces with a SiC abrasive sampling stick and the scrapings were analyzed on SiC substrate. The samples of corrosion products were directly collected from post surfaces and, before the analysis, were ground and mixed with potassium bromide. In addition, the samples collected from the surfaces of the fragments were analyzed by X-ray diffraction (XRD) technique. The XRD spectra were acquired by a Bruker D8 diffractometer (Bruker, Billerica, USA), using a Cu Ka radiation source with a 40 kV accelerating voltage and a 40 mA filament current: Θ–2Θ scans from 6° to 130° were performed, with a 0.02° step size and a 10 s dwell time.
The protectiveness of paints of the samples 1_Enna and 2_Bergamo was evaluated by electrochemical impedance spectroscopy (EIS). In order to check the reliability of the technique, EIS measurements were also performed on samples in modern gray cast iron (plates 5.5 x 10 cm in size, approximately), subjected to the current standard painting cycle (thickness about 200 µm) of Neri S.p.A. (Longiano, FC, Italy). The modern gray cast iron samples were monitored by collecting EIS spectra during exposure to neutral salt spray test (5% sodium chloride dissolved in deionized water), after 15, 42 and 83 days (corresponding to 360, 1000 and 2000 hours). The tests were performed by using an EIS probe for in situ electrochemical characterization of coatings on outdoor real components and structures (similar to that already used in [19]), that was placed in contact with the samples by interposing a cloth soaked with a natural mineral water having constant conductivity (222 µS·cm^{-1} at 20 °C). The spectra were recorded after about 20 min monitoring of the open circuit potential (E_{OCP}), when the E_{OCP} variations were lower than 2 mV/10 min. For these tests, a PAR EG&G 273A potentiostat (Princeton Applied Research, Princeton, USA) was used, coupled with a FRA Solartron 1260 frequency response analyzer (Ametek, Berwyn, USA), under the following experimental conditions: ±10 mV rms alternating potential signal; 1MHz – 1 mHz frequency range.

RESULTS

Microstructural characterization

The optical micrographs of the microstructure observed on the cross sections of cast irons before chemical etching are shown in Fig. 1. In accordance with the standard EN ISO 945-1:2008, samples 1_Enna (Fig. 1a), 2_Bergamo (Fig. 1b) and 3_Imola (Fig. 1c) were characterized by lamellar graphite of Type B (rosette grouping with random orientation). For samples 1_Enna and 2_Bergamo, the graphite lamellae were between 0.12 and 0.25 mm in length, while on sample 3_Imola lamellae lengths in the range of 0.06 and 0.12 mm were measured. The sample 4_Nice (Fig. 1d) showed Type D lamellar graphite (fine, randomly oriented graphite flakes in the interdendritic position) with length shorter than 0.015 mm.

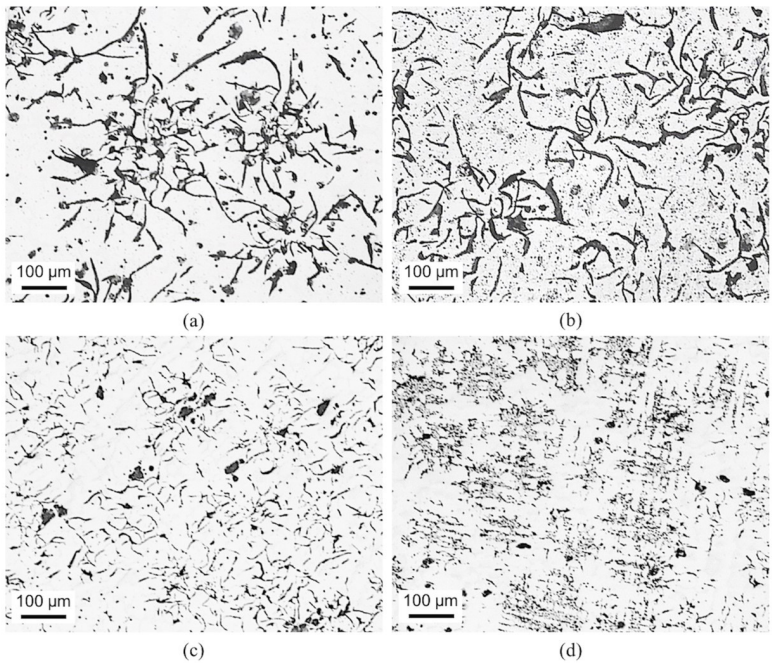

Fig. 1 – Optical micrographs of the microstructure observed on the cross sections of cast irons before chemical etching: (a) sample 1_Enna; (b) sample 2_Bergamo; (c) sample 3_Imola; (d) sample 4_Nice. / *Micrografie ottiche rappresentative della microstruttura delle ghise in sezione trasversale ed in assenza di attacco metallografico: (a) campione 1_ Enna; (b) campione 2_Bergamo; (c) campione 3_Imola; (d) campione 4_Nice.*

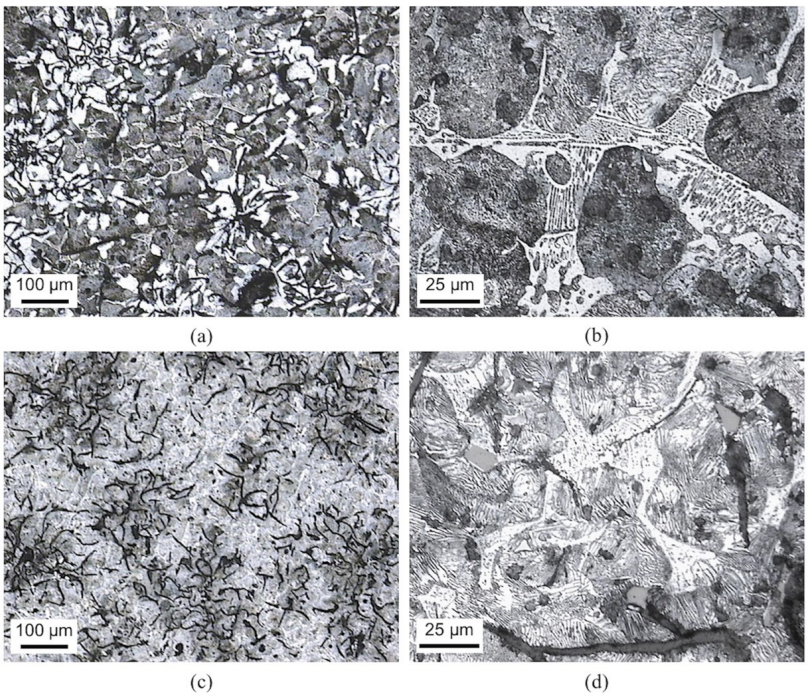

Fig. 2 – Optical micrographs of the microstructure observed on the cross sections of sample 1_Enna (a, b) and sample 2_Bergamo (c, d), after chemical etching. / *Micrografie ottiche rappresentative della microstruttura dei campioni 1_Enna (a, b) e 2_Bergamo (c, d) in sezione trasversale e dopo attacco metallografico.*

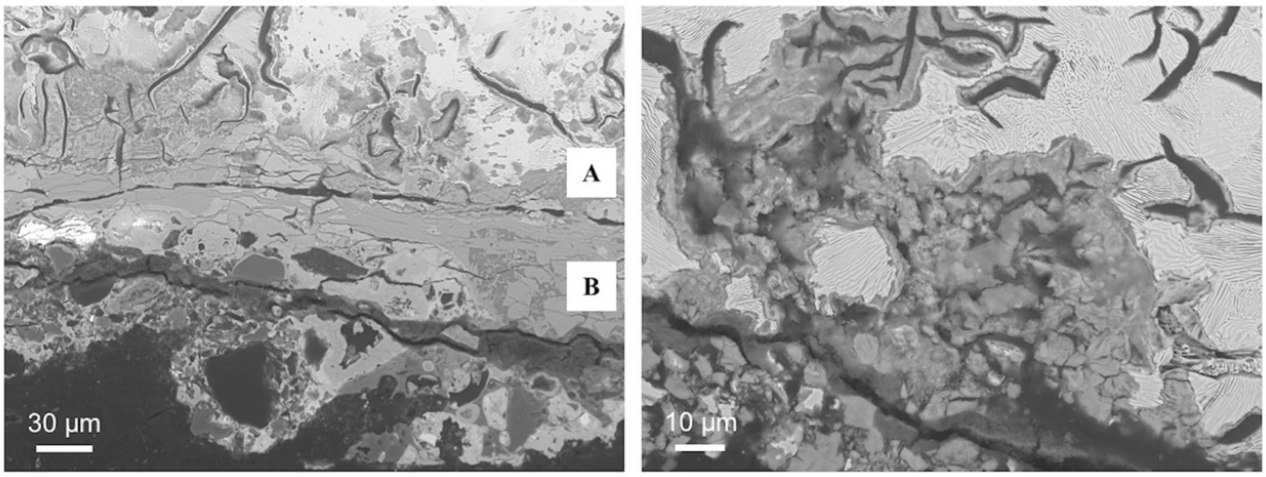

Fig. 3 – VPSEM backscattered electron images of the cross section of the corrosion patina, observed on the surface of the sample 2_Bergamo: (a) overview of the patina; (b) detail of the inner layer. / *Micrografie VPSEM in modalità elettroni retrodiffusi rappresentative della patina di corrosione osservata sulla superficie del campione 2_Bergamo: (a) visione generale della patina di corrosione; (b) dettaglio dello strato interno di corrosione.*

Fig. 2 shows the optical micrographs of 1_Enna and 2_Bergamo cross sections after chemical etching. In the first case (Fig. 2a and b), the microstructure was characterized by the presence of pearlite, ferrite close to the graphite rosettes (white areas in Fig. 2a), steadite (eutectic of iron phosphide Fe_3P and iron, Fig. 2b), and impurities in the form of polygonal shape particles. The semi-quantitative EDS analyses highlighted that the amounts of sulfur and manganese detected in these polygonal shape particles were higher than in the metal matrix. In the 2_Bergamo sample (Fig. 2c and d), characterized by a pearlitic microstructure with uniformly distributed steadite, a higher amount of impurities than that observed on the cross section of the sample 1_Enna was detected. The microstructures of the cross sections of samples 3_Imola and 4_Nice were similar to that of the sample 2_Bergamo, but with very few impurities.

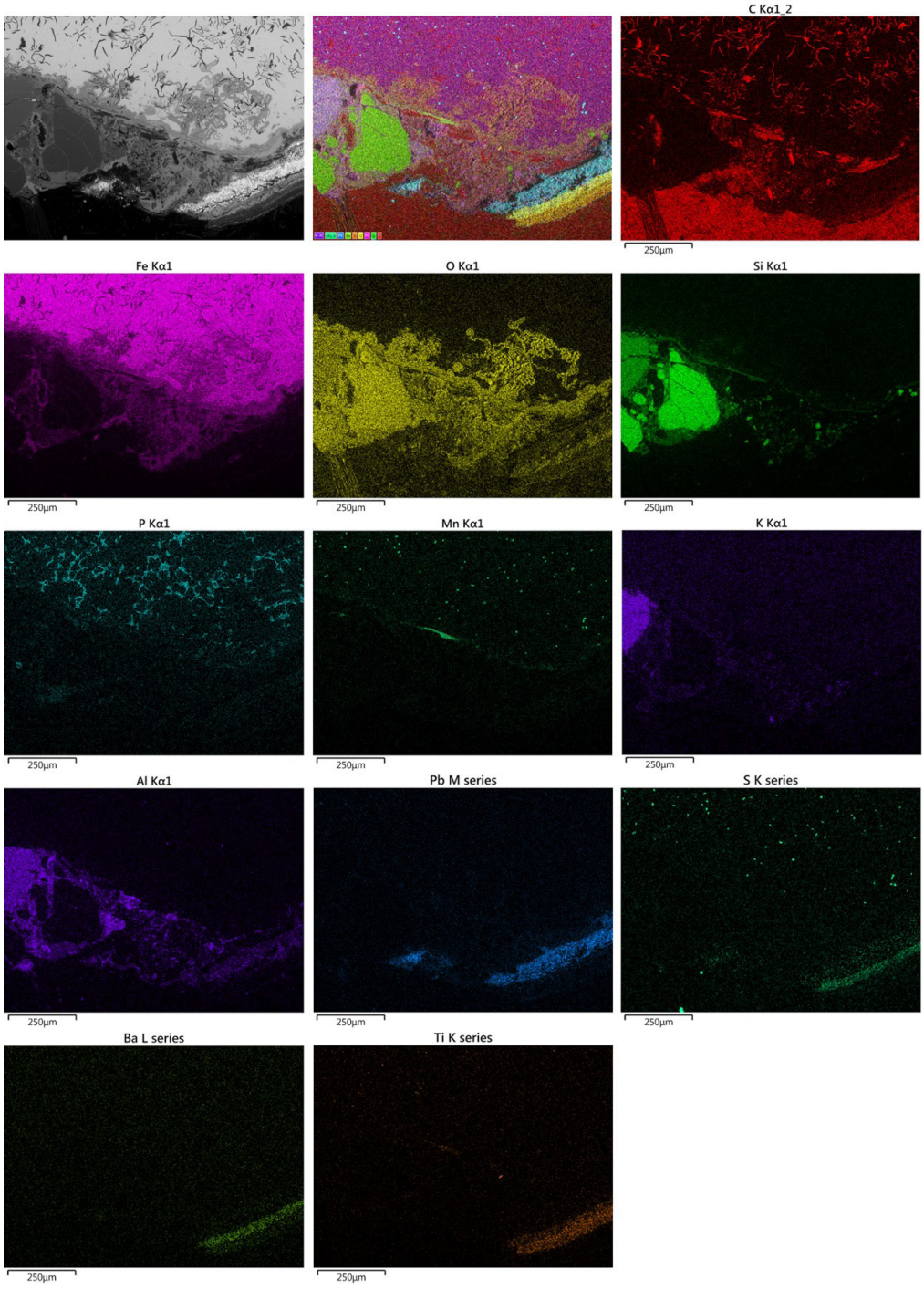

Fig. 4 – VPSEM backscattered electron images (upper left corner), layered image of X-ray maps (upper center) and maps of elemental distribution in the cross section of the sample 3_Imola. / *Micrografia VPSEM in modalità elettroni retrodiffusi (in alto a sinistra), sovrapposizione di mappe di raggi X (in alto al centro) e mappe rappresentative della distribuzione degli elementi chimici nella sezione trasversale del campione 3_Imola.*

Characterization of the corrosion phenomena

An example of the stratigraphy of the corrosion patina observed on the surfaces of the examined cast irons is shown in the VPSEM backscattered electron images of Fig. 3. Two distinct layers of corrosion products were recognizable: an inner layer (indicated by letter A in Fig. 3a) characterized by non-uniform penetration inside the less noble alloy phase (Fig. 3b), and an external one on the top (indicated by letter B in Fig. 3a).

The VPSEM/EDS mapping of the corrosion patina and paint on the cross section of the sample 3_Imola is reported in Fig. 4. The EDS maps measured on the inner layer of corrosion suggested that the selective attack of the matrix essentially produced iron corrosion products. Inside the outer corrosion layer, iron oxides were visible, admixed with elements from the corrosive environment (e.g. K and Al from particulate matter). The EDS maps also highlighted that the corrosion patina was overlain by a multilayer paint. Beginning from the outer corrosion layer, the paint was composed of a Pb-rich layer, a S- and Ba-rich layer, and a Ti-rich layer. The VPSEM/EDS mapping performed on the sample 2_Bergamo showed that the stratification of the corrosion products and paint was similar to that observed on sample 3_Imola. In the 1_Enna and 4_Nice samples the EDS maps on the layers of corrosion products were similar to those in Fig. 4. However, in the paint layer of 1_Enna sample only Ba-, S- and O-rich particles (likely $BaSO_4$) were detected, whereas Zn-rich particles were identified in the paint layer of the sample 4_Nice.

The FT-IR spectra of the paint samples are showed in Fig. 5a. The paints spectra were complicated by the presence of additional components in the paint formulation, such as the pigments, extenders and dryers that exhibited their specific absorption peaks, making the identification of the paints a complex task. In all spectra the typical vibration of aliphatic functional groups was present, related to symmetric and asymmetric C-H stretching and C-H deformation bands (occurring respectively at 2926 cm^{-1} and 2856 cm^{-1} and at 1452-1413 cm^{-1}) and a large band centered around 3400 cm^{-1} related to OH stretching. The samples 1_Enna and 2_Bergamo showed a strong and intense peak at 1733 cm^{-1} related to the stretching of the carbonyl group. In addition to a strong band present in the region 1285-1175 cm^{-1} involving the stretching of the carboxylic group bonds, a further IR band near 1030 cm^{-1}, related to the stretching of O-C bond in the $O\text{-}CH_2$ group, was observed. These findings suggested that these coatings were alkyd resins. The sample 2_Bergamo Red Layer collected from the layer beneath the paint, showed, in the low energy portion of the spectrum, three peaks at 550, 529 and 429 cm^{-1} related to the presence of minium (Pb_3O_4).

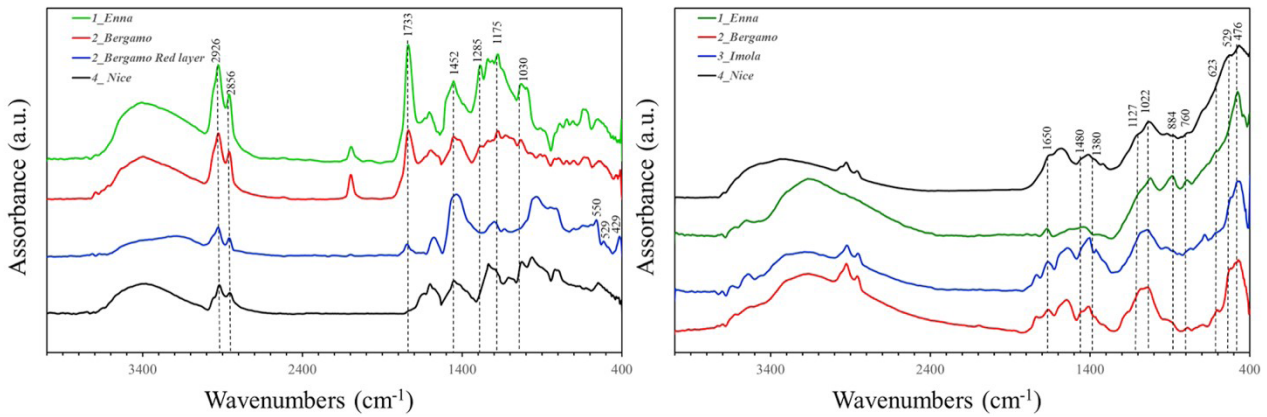

Fig. 5 – FT-IR spectra of (a) paints and (b) corrosion products collected on post-mounted luminaries exposed outdoor. / *Spettri FT-IR relativi alle vernici (a) e ai prodotti di corrosione (b), visibili sulla superfice dei lampioni oggetto di studio.*

In Fig. 5b, the FT-IR spectra collected on the corrosion products scraped from the post surfaces are reported. All the spectra appeared quite similar: the peak at 1022 cm^{-1} and the shoulder at 1127 cm^{-1} were related to the in plane Fe-O-H bending, while the peaks at 760 and 476 cm^{-1} were related to the out of plane Fe-O-H bending. All these characteristic peaks indicated the presence of lepidocrocite (γ-FeOOH) [21,22] in all the samples. The peaks at 884 and 623 cm^{-1} also suggested the occurrence of a small amount of goethite (α-FeOOH) [21,22]. The large band in the range 3100-3600 cm^{-1} was related to OH stretching of hydroxyl groups of both goethite and lepidocrocite, but it was also probably related to the vibration of water in crystal structure, as confirmed by the presence of a shoulder at 1650 cm^{-1}. The shoulder detected at 529 cm^{-1} on the samples 1_Enna, 2_Bergamo and 4_Nice could be related to the presence of minium, but the XRD spectra highlighted the presence of the crystalline form of this compound, together with anatase (TiO_2), only in the samples 2_Bergamo and 3_Imola. The spectra also indicated the presence of some organic compounds (band at 2800-3000 cm^{-1} and peaks around at 1480 and 1380 cm^{-1}) probably due to the deposition of organic substances or to the residues of the original paint.

In all samples, the VPSEM/EDS observations highlighted the presence of both flower-like pattern and the foam-like morphology of the lepidocrocite (Fig. 6a), and the cloudy or cotton-ball-like microstructure associated to the goethite (Fig. 6b).

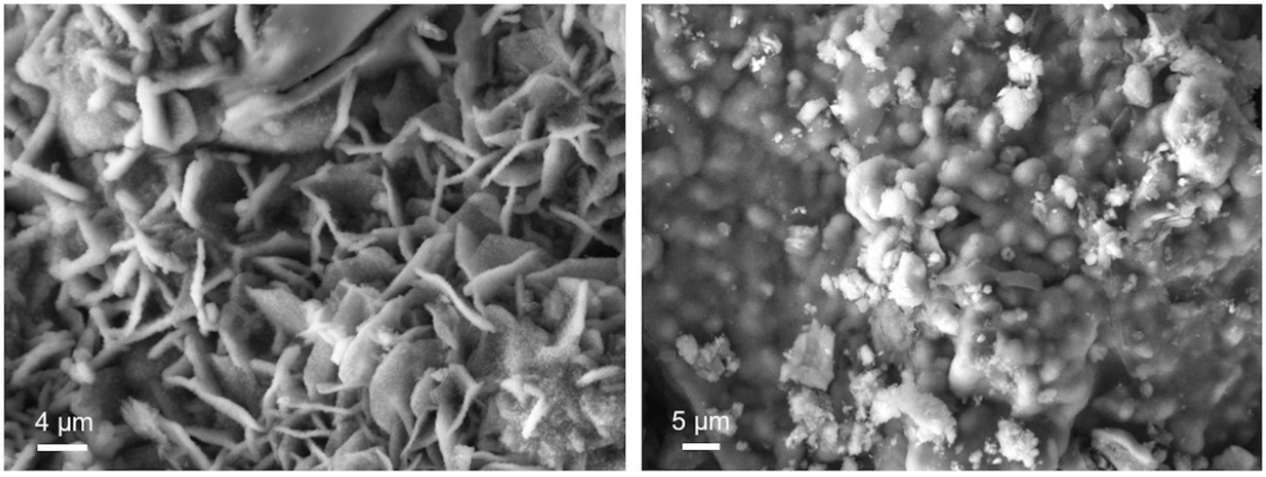

Fig. 6 – VPSEM images of the corrosion products observed on the surface of the examined samples: (a) detail of lepidocrocite; (b) detail of goethite. / *Micrografie VPSEM rappresentative dei prodotti di corrosione osservati sulla superfice dei campioni indagati: (a) dettaglio della lepidocrocite; (b) dettaglio della goethite.*

Electrochemical characterization

Fig. 7 shows the EIS spectra in Nyquist format, recorded on 1_Enna and 2_Bergamo samples (carrying the original paint layers, Fig. 7a) and on the plates in modern gray cast iron with the standard Neri S.p.A. coating (Fig. 7b), the latter after 15, 42 and 83 days of exposure to the salt spray test.

The EIS spectra mainly showed two time constants: the high frequency (HF) one corresponds to the semicircle at frequencies higher than 10^3 Hz (for the ancient samples) or 10^1 Hz (for the modern one) and the low frequency (LF) one is related to the arc at frequencies lower than 1 Hz (for the ancient samples) or 10^{-1} Hz (for the modern one). For a defective organic coating [23,24], the HF time constant is linked to the porous coating properties, while the LF one to the charge transfer at the bottom of the coating pores. In the case of the sample 2_Bergamo also a third time constant was detectable at intermediate frequencies (around 10^2 Hz), which could be related to the dielectric properties of the corrosion product layer formed underneath the protective coating [25,26]. The shape of the spectrum of 1_Enna sample did not exclude that this time constant was also present but overlapped to the LF one.

The HF range of the EIS spectra related to the coating dielectric properties were analyzed by using a simple parallel R-C circuit, to evaluate the coating pore resistance, R_{pore}, and the coating capacitance, C_c [25]. The corrosion behavior of the metal substrate was evaluated by estimating the polarization resistance value, R_p, as the limit of the LF capacitive semicircle for frequency tending to 0. R_p is known to be inversely proportional to the corrosion rate [25]. All the obtained parameters are reported in Table 2. For the modern gray cast iron sample exposed to the salt spray test for 15 days, the second semicircle in the Nyquist plot was characterized by too few scattered data, thus the R_p value was not evaluated.

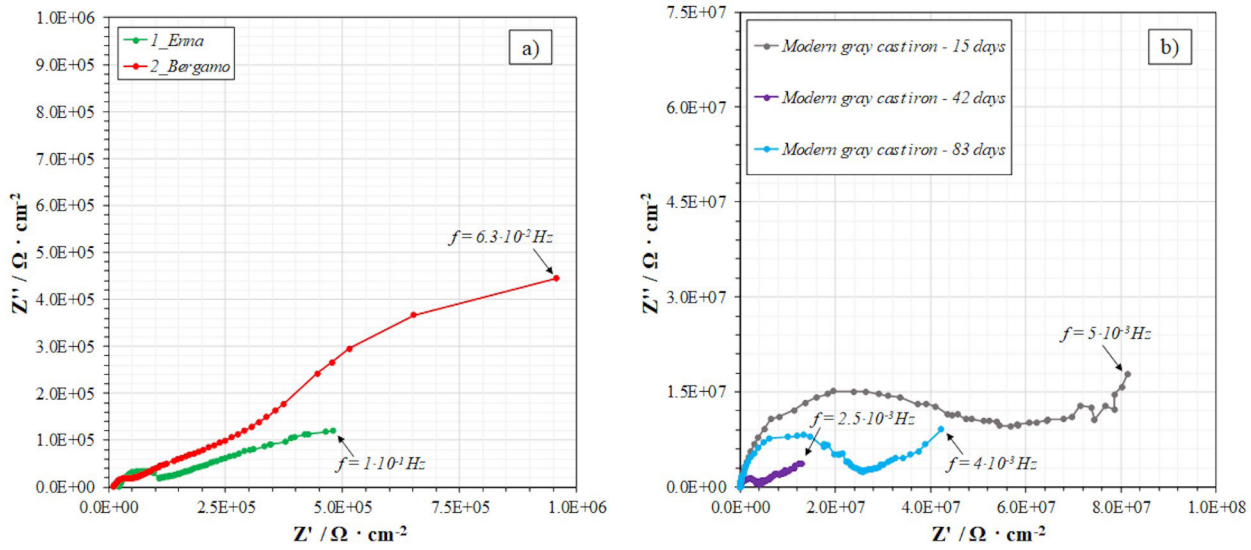

Fig. 7 – EIS spectra in Nyquist format, recorded on (a) 1_Enna and 2_Bergamo samples and on the plates in modern gray cast iron (b). / *Spettri EIS, sotto forma di diagrammi di Nyquist, registrati (a) sui campioni 1_Enna e 2_Bergamo, e sulle lastrine in ghisa grigia moderna (b).*

Tab. 2 – Values of R_{pore} (Ω·cm²), C_c (F·cm⁻²) and R_p (Ω·cm²) obtained from EIS fitting with the adopted equivalent circuit. / *Valori di R_{pore} (Ω·cm²), C_c (F·cm⁻²) e R_p (Ω·cm²) ottenuti dopo fitting dei dati EIS mediante il circuito equivalente adottato.*

Sample	R_{pore} (Ω·cm²)	C_c (F·cm⁻²)	R_p (Ω·cm²)
Modern gray cast iron after 15 days in salt spray test	$3.9 \cdot 10^{7}$	$1.7 \cdot 10^{-10}$	-
Modern gray cast iron after 83 days in salt spray test	$2.1 \cdot 10^{7}$	$2.0 \cdot 10^{-10}$	$9.8 \cdot 10^{7}$
1_Enna	$6.3 \cdot 10^{4}$	$7.0 \cdot 10^{-11}$	$2.4 \cdot 10^{6}$
2_Bergamo	$4.0 \cdot 10^{4}$	$1.7 \cdot 10^{-10}$	$2.6 \cdot 10^{6}$

R_{pore} values of the coating on the modern gray cast iron remained higher than 10^7 $\Omega \cdot cm^2$ until the end of the exposure to the salt spray test. The corresponding C_c values only slightly increased during the test indicating that it offered a high barrier effect against water absorption [27]. R_{pore} values of the ancient paints were more than two orders of magnitude lower than those of the modern one, suggesting that they were affected by many pores and cracks. The C_c value of 1_Enna sample was smaller than those measured on the modern paint, while that of 2_Bergamo was equal. Capacitances are proportional to the dielectric constant of the coatings (ε) and inversely proportional to their thickness. Dry conditions are present in both ancient paints, due to their persistence in indoor conditions for many years and due to the short measurement time in contact with mineral water. These conditions induce low coating ε values and justify the low C_c value measured on 1_Enna sample, as this ancient and the modern coatings have comparable thickness. In the case of 2_Bergamo, C_c is comparable to those measured on the modern paint and this could be connected to the lower coating thickness. The estimated R_p values of the ancient samples were more than one order of magnitude lower than that on modern gray cast iron at the end of salt spray test exposure, evidencing the higher corrosion rates of the underlying metal due to the scarce residual protectiveness of the ancient coatings.

DISCUSSION

This work evaluates the conservation state of European street furniture in painted and partially corroded cast iron artefacts. All examined cast irons can be classified as gray cast irons. The distribution of the lamellar graphite of Type B in samples 1_Enna, 2_Bergamo and 3_Imola is frequently encountered on alloys solidified with an intermediate degree of undercooling, whereas the distribution of type D and the very fine graphite lamellae of the sample 4_Nice forms typically under a relatively high degree of undercooling [28]. All metalworks show microstructures with high steadite contents. It is known that the presence of steadite is due to the addition of phosphorus. This element lowers the melting point and improves the fluidity of cast iron alloys, thus favoring the manufacturing of complex shape castings with thin wall thickness (e.g. castings for European street furniture) [28].
The study of the patina stratification, the main corrosion products and corrosion attack morphology suggests that a specific corrosion phenomenon occurred. In an outdoor environment, where paints are partially removed and/or damaged, acidic rainwater starts to corrode cast iron alloys. As the ferrous matrix corrodes, the more noble graphite further promotes the attack of the surrounding metal by the galvanic coupling effect. The graphitic corrosion residue is impregnated with corrosion products of iron: lepidocrocite, characterized by a flower-like pattern and a foam-like morphology, and goethite with a cloudy or cotton-ball-like microstructure (as identified by FT-IR and VPSEM/EDS). The affected surfaces show a compact layer of graphite, rust and impurities (as confirmed by the scanning electron microscope observations), that may inhibit further damage. The cast iron elements retain their appearance and shape, but undergo a mechanical weakening. This phenomenon is referred to in the literature as graphitization, graphitic or spongy corrosion [5,7,28].
The examinations of paints applied on the surfaces of cast irons indicate the use of pigments (TiO_2 and likely $BaSO_4$), alkyd resins and minium as a passivating primer layer. According to the literature, the most common coating system detected on historical ironworks was a traditional oil paint composed of turpentine solvent, linseed oil binder, pigments and additives, mainly driers. These were usually applied over a primer containing pigments: red ochre with a small proportion of white lead in the seventeenth and early eighteenth centuries, and red lead (minium) in linseed oil primers in the late eighteenth and nineteenth centuries. Red lead formed lead soaps with linseed oil, which became an elastic and tough film, impervious to water. At least two slow-drying linseed-oil based finish layers were applied over a red lead primer [7]. From the 1930s on, the most common replacement for traditional oil paints was the painting with alkyd resins. These materials provided the advantage of a higher layer thickness from one application and faster drying than the traditional oils [4].
The electrochemical characterization of paints further confirmed the capability of EIS technique in evaluating the conservation state of ancient painted artefacts [9,11,12] and the barrier property variations in modern coatings even when not detectable by visual observation [29].

CONCLUSIONS

Our study investigates the state of conservation of four painted and partially corroded post-mounted luminaries, dating back to the nineteenth and the twentieth centuries and coming from foundries located in Italy and France. The microstructure of the cast irons was consistent with the procedures employed for manufacturing complex shape casting with variable wall thickness. The Italian castings were composed of lamellar graphite of Type B and with lamellae between 0.06 and 0.25 mm in length. For the samples 2_Bergamo and 3_Imola, the microstructure was pearlitic with a high amount of steadite and manganese sulfides. The microstructure of the sample 1_Enna was similar, but with ferrite close to the graphite rosettes. The French casting had lamellar graphite of Type B, with lamellae length shorter than 0.015 mm and a microstructure similar to that of samples 2_Bergamo and 3_Imola.
The study of the patina stratification, the main corrosion products and corrosion attack morphology indicated the graphitization of cast irons. This phenomenon was accompanied by the deposition of thick layers of corrosion, containing lepidocrocite, goethite and impurities from the corrosive environment.
On the examined fragments, no historical paints were detected, suggesting the removal of the deteriorated paint layers from the surfaces, before the application of modern paint systems. Finally, the electrochemical characterization established the poor protectiveness offered by the paints on the post-mounted luminaries.

ACKNOWLEDGEMENTS
Dr Raffaella Bassi Neri and Dr Antonio Neri, NERI Foundation – The Italian Museum of Cast Iron (Longiano, FC, Italy), are gratefully acknowledged for providing the cast iron artefacts investigated in the present work.

REFERENCES

[1] R. Bassi, L. Bazzocchi, Cast iron artefacts for city décor: a list of the principal typologies, in: So light and yet a metal – The art of cast iron in the 19th and 20th centuries, R. Bassi, C. Biasini Selvaggi, M.G. Massafra (Eds.), Barbieri Selvaggi Editori, Manduria, 2011, p. 33–34.
[2] R. Bassi Neri, La ghisa: quando il gusto incontrò l'arte industriale, Arredo&Città, 2 (2011) 5.
[3] J. Gay, Cast iron: Architecture and ornament, Function and Fantasy, John Murray Publishers Ltd., London, 1985.
[4] S. Godfrain, R. Pender, B. Martin, English Heritage – Practical building conservation – Metals, Ashgate Publishing Limited, Farnham, 2012.
[5] A. Reynaud, Corrosion of cast irons, in: Sheir's Corrosion – Corrosion and degradation of engineering materials, vol. 3, B. Cottis, M. Graham, R. Lindsay, S. Lyon, T. Richardson, D. Scantlebury, H. Stott (Eds.), Elsevier Ltd., Amsterdam, 2010, p. 1737–1788.
[6] P. Dillmann, D. Watkinson, E. Angelini, A. Adriaens, Corrosion and conservation of cultural heritage metallic artefacts, Woodhead Publishing, Cambridge, 2013.
[7] K. Kreislova, D. Knotkova, H. Geiplova, Atmospheric corrosion of historical industrial structures, in: Corrosion and conservation of cultural heritage metallic artefacts, P. Dillmann, D. Watkinson, E. Angelini, A. Adriaens (Eds.), Wood head Publishing, Cambridge, 2013, p. 311–343.
[8] X.X. Fu, J.H. Dong, E.H. Han, W. Ke, A new experimental method for in situ corrosion monitoring under alternate wet–dry conditions, Sensors 9 (2009) 10400–10410.
[9] C. Li, Y. Ma, Y. Li, F. Wang, EIS monitoring study of atmospheric corrosion under variable relative humidity Corros. Sci. 52 (2010) 3677–3686.
[10] C. Thee, L. Hao, J. Dong, X. Mu, X. Wei, X. Li, W. Ke, Atmospheric corrosion monitoring of a weathering steel under an electrolyte film in cyclic wet–dry condition, Corros. Sci. 78 (2014) 130–137.
[11] E. Angelini, D. Assante, S. Grassini, M. Parvis, EIS measurements for the assessment of the conservation state of metallic works of art, Int. J. Circ., Syst. Signal Process. 8 (2014) 240–245.
[12] S. Grassini, S. Corbellini, M. Parvis, E. Angelini, F. Zucchi, A simple Arduino-based EIS system for in situ corrosion monitoring of metallic works of art, Measurement 114 (2018) 508–514.
[13] F. Mansfeld, Use of electrochemical impedance spectroscopy for the study of corrosion products protection by polymer coatings, J. Appl. Electrochem. 25 (1995) 187–202.
[14] A. Nishikata, Y. Ichihara, T. Tsuru, An application of electrochemical impedance spectroscopy to atmospheric corrosion study, Corros. Sci. 37 (1995) 897–911.
[15] A. Nishikata, Y. Yamashita, H. Isatayama, T. Tsuru, A. Usami, K. Tanabe, H. Mabuchi, An electrochemical impedance study on atmospheric corrosion of steels in a cyclic wet-dry condition, Corros. Sci., 37 (1995) 2059–2069.
[16] A. Nishikata, F. Suzuki, T. Tsuru, Corrosion monitoring of nickel-containing steels in marine atmospheric environment, Corros. Sci., 47 (2005) 2578–2588.
[17] P. Letardi, Use of electrochemical impedance spectroscopy on outdoor bronze monuments, CSA, EAS06, 13-14 No vember 2006, Somerset, USA.
[18] P. Letardi, Laboratory and field tests on patinas and protective coating systems for outdoor bronze monuments, Pro ceedings of Metal 2004, 4–8 October 2004, National Museum of Australia, Canberra ACT (Australia), p. 379–387.
[19] A. Balbo, M. Abbottoni, A. Frignani, C. Chiavari, C. Martini, E. Bernardi, C. Monticelli, In-situ EIS characterization of outdoor corrosion behaviour of bronze and gilded bronze, EUROCORR 2014, European Federation of Corrosion Event No. 364, 8-12 September 2014, Pisa, Italy, Paper 7259, p. 1–9.
[20] S.S. Jamali, Y. Zhao, Z. Gao, H, Li, A.C. Hee, In situ evaluation of corrosion damage using non-destructive electrochemical measurements. A case study, J. Ind. Eng. Chem. 43 (2016) 36–43.
[21] S. Rahimi, R M Moattari, L Rajabi, A Ashraf Derakhshan, M. Keyhani, Iron oxide/hydroxide (α,γ-FeOOH) nanoparticles as high potential adsorbents for lead removal from polluted aquatic media, J. Ind. Eng. Chem. 23 (2015) 33–43.
[22] T. Ishikawa, Y. Kondo, A. Yasukawa, K. Kandori, Formation of magnetite in the presence of ferric oxyhydroxides, Corros. Sci. 40 (1998) 1239–1251.

[23] J. N. Murray, Electrochemical test methods for evaluating organic coatings on metals: an update. Part III: Multiple test parameter measurements, Prog. Org. Coat. 31 (1997) 375–391.
[24] A. Lasia, Electrochemical impedance spectroscopy and its application, Springer Science + Business Media, New York, 2014.
[25] G. Trabanelli, C. Monticelli, V. Grassi, A. Frignani, Electrochemical study on inhibitors of rebar corrosion in carbonated con crete, Cement Concrete Res. 35 (2005) 1804–1813.
[26] C. Zhang, J. Zhao, Effects of pre-corrosion on the corrosion inhibition performance of three inhibitors on Q235 steel in CO_2/H_2S saturated brine solution, Int. J. Electrochem. Sci. 12 (2017) 9161–9179.
[27] J. Gonzalez-Guzman, J.J. Santana, S. Gonzalez, R. M. Souto, Resistance of metallic substrates protected by organic coating containing glass flakes, Prog. Org. Coat. 68 (2010) 240–243.
[28] ASM Specialty Handbook, Cast Irons, ASM International, Materials Park, Ohio, 1996.
[29] F. Deflorian, S. Rossi, L. Fedrizzi, P.L. Bonora, Testing of protective organic coatings on metals: comparison of salt spray and electrochemical impedance spectroscopy, J. Test. Eval. 31 (2) (2003) 91–97.